HiSST: 3rd International Conference on
High-Speed Vehicle Science Technology
14 -19 April 2024, Busan, Korea

Investigation of mixing and Combustion in supersonic flows

Sasi Kiran Palateerdham [1], L N Phaneendra Peri [2], Antonella Ingenito [3], Gautam Choubey [4]

Abstract

The significance of green transportation at hypersonic speeds is the current field of research for space launchers and commercial trans atmospheric vehicles. However, due to their high speeds at Mach > 1, results in a very short residence time of the order of few milliseconds (10^{-3} – 10^{-4} s) minimizing the chances for air-fuel barely mix and burn. Furthermore, the interaction of fuel injection at sonic speed via transverse and cross flow with incoming airstream at high Mach results in the generation of complex vortices that effect the chemical kinematics and combustion and are influenced by the dilatational term "∇.U". therefore, the supersonic combustion region is affected by compressibility and the corresponding baroclinic terms. Thus, it is very important to realize the behavior of flow while different injection angles, the geometry of the cavity and the corresponding flow behavior. This could be realized by the numerical simulation of flow to better understand the physics of supersonic combustion. Therefore, the current study plans to understand the shock and how it interacts with fuel injection and mixing, the resulting vorticity development, the effects of adding heat and boundary layer separation on total pressure loss by utilizing large eddy simulations.

Keywords : Supersonic Flow, Scramjet, Aerospace, Combustion, Propulsion

Nomenclature

C_p	Specific heat at constant pressure (J/Kg. K)
d	Injector diameter (m)
E	Total specific energy (J/kg)
k	Turbulent kinetic energy
Le	Lewis number
Ma	Mach number
Pr	Prandtl number
p	Pressure (Pa)
S	Source-term vector
t	Time variable
T	Temperature (k)
U	Vector of conserved variables
u_j	Velocity (m/s)
U	Inflow velocity (m/s)
Z	Mixture fraction
n	time step

Greek letters

ρ	Density ($Kg.m^{-3}$)
μ	Molecular viscosity ($Kg.m^{-1}.s^{-1}$)
$\Re_u$	Universal gas constant (J/(K·mol))
τ_{ij}	Viscous stress tensor

[1] *PhD student, Scuola di Ingegneria Aerospaziale, Sapienza University of Rome, 00138, Italy, sasikiran.palateerdham@uniroma1.it*
[2] *PhD student, Scuola di Ingegneria Aerospaziale, Sapienza University of Rome, 00138, Italy, phanindra.p123@gmail.com*
[3] *Professor (Associate), Scuola di Ingegneria Aerospaziale, Sapienza University of Rome, 00138, Italy, antonella.ingenito@uniroma1.it*
[4] *Professor (Assistant), Department of Mechanical Engineering, National Institute of Technology (NIT) Silchar Assam 788010, India. gautamchoubey@mech.nits.ac.in*

1. Introduction

The use of hypersonic propulsion in aviation and aerospace applications is certainly a promising alternative for green and fast propulsive systems [1]. A scramjet engine, which is regarded as a favorable airbreathing engine, has the potential for hypersonic applications [2]. However, their operation in harsh environments with high-speed intake makes their operating conditions critical. The scramjet intake must accommodate the flow field, which remains to be supersonic and poses a significant challenge. The combustion phenomena in supersonic flow are featured by a wide variety of interactions resulting from injector flows, shock waves, boundary layers and cavity flows.

There are challenges encountered for Mixing of reactants, ignition, flame holding and completion of combustion due to short resident time [3]. In flight conditions of Mach > 10, the temperatures in the combustor are significantly high enough for the auto-ignition of fuel. However, in low Mach conditions (M < 5), this can be more critical due to low temperatures at the intake. The problem is worsened further in the case of liquid fuels due to the intricacy of fuel injection, molecular mixing, and atomization and vaporization [4-5]. Researchers across the world, working on different methods and techniques to increase the residual time and mixing. There are wide varieties of techniques implemented in the scramjet combustor for flame holding [8]. Implementation of different struts [9], cavities [10], ramps [11] etc. in the combustor can be found in the literature and these methods have shown an improvement in combustor performance. among all, Cavity based combustors showed a significance amount of increase in mixing and residual time for the scramjet. Also, they are passive in nature and simple in design.

The present study aims to investigate the effect of shock development and interaction with the mainstream, the development of vorticity and its effects in combustion [12]. To answer these questions, we have made a study using RANS/LES on a cavity-based scramjet. Analysis of the LES simulation of the HIFiRE-2 scramjet revealed the direct and mutual effects of the shock waves' interaction with vorticity, the addition of heat, friction, mixing, and boundary layer separation on the total pressure loss. Consequently, by looking at the temporal progression of the iso-surfaces, it becomes possible to observe the development of vortices and discern whether the deformation of a fluid element primarily stems from the strength of rotation or the strain that directly influences the elongation of the vortex tube in subsonic flows.

2. Theory of the Turbulence Combustion in Supersonic flow

2.1. Physical insight into the Supersonic flow and combustion

In supersonic flow, the nature of the turbulence, the corresponding vorticity and the consequent helicity which effects the fuel mixing is highly influenced by the Mach flow conditions, the influence of these parameters can be given by the dimensionless vorticity equation for compressible flows as:

$$\underbrace{\frac{\partial \bar{\omega}}{\partial t}}_{\text{Inertia}} + \underbrace{(\bar{u}\cdot\bar{\nabla})\bar{\omega}}_{\text{Convection}} = \underbrace{\bar{\omega}\cdot\overline{\nabla u}}_{\text{compressibility}} - \underbrace{\bar{\omega}(\bar{\nabla}\cdot\bar{u})}_{\text{Vortex-stretching}} + \underbrace{\frac{\overline{\nabla\rho}\times\overline{\nabla p}}{\rho^2}}_{\text{Baroclinic}} + \underbrace{\frac{1}{Re}\nu\overline{\nabla^2\omega}}_{\text{diffusion}}$$

$$+\frac{1}{Re}\Bigg(\underbrace{-\frac{1}{\rho^2}\overline{\nabla\rho}\times(\bar{\nabla}\cdot\bar{\sigma})}_{\text{Compressibility-vorticity}} + \underbrace{\frac{1}{\rho}\left\{\overline{\nabla\mu}\times\left[\overline{\nabla^2 u}+\bar{\nabla}(\bar{\nabla}\cdot\bar{u})\right]\right.}_{\text{vorticity-vorticity}} + \underbrace{\left.2\bar{\nabla}\times\left(\bar{\bar{E}}\overline{\nabla\mu}\right)\right\}}_{\text{strain-vorticity}}\Bigg)$$

From the equation, it can be inferred that in supersonic flows, the convective term (2nd term), baroclinic term (3rd term), vortex stretching term (4th term), and compression term (5th term) exhibit comparable magnitudes and consequently exert similar effects on the flow, whether at large or small scales. The convective term $\bar{\omega}\left(\bar{\nabla}\cdot\bar{u}\right)$ appears only in compressible flows. Depending on the presence of local compressions or expansions, this term has the capacity to either concentrate or disperse vorticity

throughout the field. On the other hand, the baroclinic term $\frac{\overline{\nabla\rho}\times\overline{\nabla p}}{\rho^2}$ signifies the generation of vorticity due to the gradients of pressure and density within the medium. Due to the pressure field and density variations in supersonic flow, regions with lower density experience greater acceleration. During this period, the baroclinic effect can either serve as a source or a sink for vorticity. The viscous terms, on the other hand, are inversely proportional to the Reynolds number, and thus, at larger scales, they become negligible. The mixing of the fuel with the incoming flow, which is largely controlled by the generation of high streamwise vorticity in the cavity, is a significant component of supersonic combustion. As for the remaining terms, they represent the influence of viscous dissipation, primarily responsible for dissipating the energy contained within vortex structures, effectively dissipating them.

Nevertheless, it is important to bear in mind that, in certain scenarios, these terms may also act as sources for vorticity. When a fuel with sonic velocity is injected into the incoming flow, a strong bow shocks occurs in the upstream region of the flow creates a strong baroclinic torque and increasing vorticity in the flow. This also leads to the loss of stagnation pressure resulting in a less efficient combustor design [7]. In this context, the authors aim to analyse the characteristics of turbulence in compressible flow, by means of a theoretical analysis and to validate this analysis by means of large eddies numerical simulations of the HIFiRE test case.

3. Governing Equations

In Numerical Modelling, the balance governing equations for the LES for conservation of mass, momentum, energy and species transport are expressed as:

Equation of Mass Conservation

$$\frac{\partial\bar{\rho}}{\partial t}+\frac{\partial\bar{\rho}\widetilde{u_i}}{\partial x_i}=0 \qquad \text{Eq. 1}$$

Transport Equation of Momentum

$$\frac{\partial(\bar{\rho}\widetilde{u_j})}{\partial t}+\frac{\partial(\bar{\rho}\widetilde{u_i}\widetilde{u_j}+\bar{p}\delta_{ij})}{\partial x_i}=\frac{\partial\tilde{\tau}_{ij}}{\partial x_i}+\frac{\partial\tau_{ij}^{sgs}}{\partial x_i} \qquad \text{Eq. 2}$$

Transport Equation of Total Energy (internal + mechanical)

$$\frac{\partial(\bar{\rho}\widetilde{U})}{\partial t}+\frac{\partial(\bar{\rho}\tilde{u}_i\tilde{U}+\bar{p}\tilde{u}_i+\overline{q_i}-\tilde{u}_i\overline{\tau_{ij}}+H_i^{sgs}-\sigma_i^{sgs})}{\partial x_i}=0 \qquad \text{Eq.3}$$

Transport Equations for the Ns species mass fractions

$$\frac{\partial(\bar{\rho}\tilde{Y}_n)}{\partial t}+\frac{\partial(\bar{\rho}\tilde{u}_j\tilde{Y}_n)}{\partial x_i}=\frac{\partial}{\partial x_i}\left[\bar{\rho}(D_n+D_{t,n})\frac{\partial\tilde{Y}_n}{\partial x_i}\right]+\bar{\rho}\widetilde{\dot{\omega}}_n \qquad \text{Eq. 4}$$

Thermodynamic Equation of State

$$\bar{p}=\bar{\rho}\sum_{i=1}^{N_s}\frac{\tilde{Y}_i}{W_i}\mathcal{R}_u\tilde{T} \qquad \text{Eq.5}$$

These equations must be coupled with the constitutive equations which describe the molecular transport. In the above equations, t is the time variable, ρ the density, uj the velocities, t_{ij} the viscous stress tensor, and $\widetilde{U}$ the total filtered energy per unit of mass, that is sum of the filtered internal energy, $\widetilde{e}$, the resolved kinetic energy, $1/2(\widetilde{u_i u_i}-\widetilde{u}_i\widetilde{u}_i)$, and the subgrid one, $1/2(\widetilde{u_i u_i}-\widetilde{u}_i\widetilde{u}_i)$, qi is the heat flux, p the pressure, T the temperature.

The stress tensor and the heat-flux are respectively:

$$\overline{\tau_{ij}} = 2\mu(\widetilde{S_{ij}} - \frac{1}{3}\widetilde{S_{kk}}\delta_{ij}) \quad \text{Eq. 6}$$

$$\bar{q}_i = -k\frac{\partial(\tilde{T})}{\partial x_i} + \bar{\rho}\sum_{n=1}^{N_s}\widetilde{h_n}\widetilde{Y_n}\widetilde{V_{i,n}} + \sum_{n=1}^{N_s} q_{i,n}^{sgs} \quad \text{Eq. 7}$$

Dn is the n[th]-species diffusion coefficient, *Wn* the n[th] species molecular weight, *Yn* the mass fraction, w_n is the production/destruction rate of species *n*, diffusing at velocity $V_{i,n}$ and resulting in a diffusive mass flux *Jn*. Finally, *Ru* is the universal gas constant. Summation of all species transport equations yields the total mass conservation equation. Therefore, the *Ns* species transport equations and the mass conservation equation are linearly dependent and one of them is redundant. Furthermore, to be consistent with mass conservation, the diffusion fluxes ($J_n = \rho Y_n V_n$) and chemical source terms must satisfy:

$$\sum_{n=1}^{N_s} J_n = 0 \quad \text{and} \quad \sum_{n=1}^{N_s} \dot{\omega}_n = 0 \quad \text{Eq.8}$$

In particular, the constraint on the summation of chemical source terms derives from mass conservation for each of the *Ns* chemical reactions of a chemical mechanism.

The sub grid scales are modelled using Smagorinsky-Lilly model. The eddy viscosity being modelled as $\nu_t = C\Delta^2\sqrt{2\bar{S}_{ij}\bar{S}_{ij}} = C\Delta^2|\bar{S}|$. Here Δ is the size of the grid and C is the constant.

4. Numerical modeling

Large Eddy Simulations were conducted using ANSYS Fluent based on version 2023 R1 by considering the governing equations and species transport equations. A density-based solver using implicit formulation and the advection upstream splitting process (AUSM) is adopted with a second-order upwind discretization technique to solve the governing equations. Gradients for convection and diffusion terms at cell faces are calculated using the least square cell-based approach, and the arithmetic mean of nearby cell centre values.

WALE sub-grid scale model was used to produce a precise solution with steady convergence characteristics to represent the effects of unresolved small-scale fluid motions (such as small eddies, swirls, vortices) in the equations governing the large-scale motions that are resolved in computer model. The Courant number is set to 0.3 to ensured standard acceptable stability (Pandey and Choubey, 2017 [13]). Mixture materials are JP-7 and air, reaction is considered as finite-rate/eddy dissipation (volumetric reaction), and density is taken as an ideal gas.

5. Geometry and boundary conditions

For numerical simulation of the flow field in the scramjet combustor, a structured grid was constructed using ANSYS Work bench. fine mesh was adopted to achieve precise results. The number of nodes is evaluated to be around 3.6 million. The inlet boundary conditions were detailed in Table 1. Normal air enters the inlet of the isolator at Mach 3.46 and the fuel is injected in sonic conditions from injectors. JP7 is considered as a fuel, which has a combination of 36% methane and 64% ethylene.

Table 1. Inflow Boundary conditions

Inflow Boundary	Pressure [KPa]	Temperature [K]	Mach
Isolator	40.3	736.2	3.46
Primary Injector	105.7	293.3	1.0
Secondary Injector	290.7	301.1	1.0

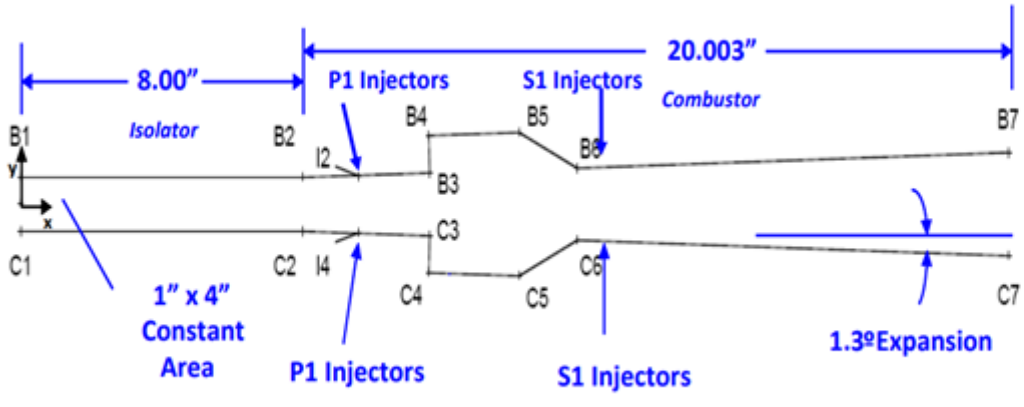

	x [mm (in.)]	y [mm (in.)]
C1	0.000	-12.7 (-0.500)
C2	203 (8.000)	-12.7 (-0.500)
C3	295 (11.596)	-14.8 (-0.582)
C4	294 (11.581)	-31.9 (-1.256)
C5	359 (14.150)	-33.4 (-1.315)
C6	401 (15.794)	17.2 (-0.677)
C7	711 (28.003)	-24.2 (-0.954)
B1	0.000	12.7 (0.500)
B2	203 (8.000)	12.7 (0.500)
B3	295 (11.596)	14.8 (0.582)
B4	294 (11.581)	31.9 (1.256)
B5	359 (14.150)	33.4 (1.315)
B6	401 (15.794)	17.2 (0.677)
B7	711 (28.003)	24.2 (0.954)
I2	244 (9.596)	13.6 (0.536)
I4	244 (9.596)	-13.6 (-0.536)

Figure 1. Schematic Diagram of the HIFiRE-2 Scramjet combustor

6. Results and discussions

The current paper investigates the flow field, vorticity, heat addition, friction, mixing, boundary layer separation and the total pressure losses in the scramjet by analysing the results at the time step t=0.0024s and the mean values. A detailed analysis of these can be further analysed by understanding the pressure, temperature, Mach, H2O contours of the simulations.

6.1. Pressure

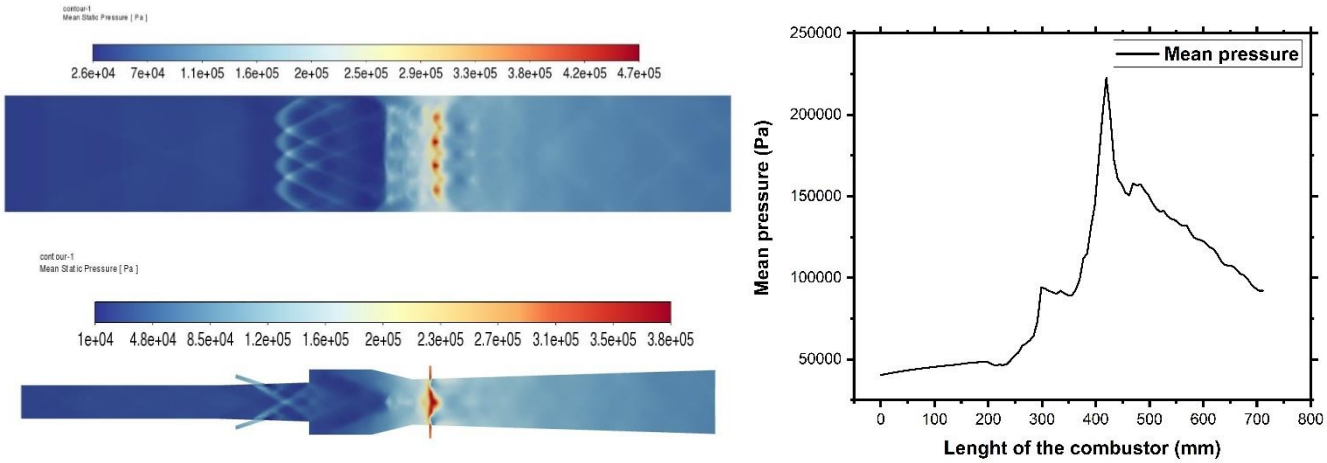

Figure 2. Contours of Pressure – Top and Front view

The results are obtained by time-averaging instantaneous flow-fields of the simulations.

Figure 2 shows the top view of the pressure contour at a distance from the wall of 0.01 m from the upper wall. Statistics from the LES are obtained by time-averaging instantaneous flow-fields after 3 flow-through times.

As a consequence of the interaction between the incoming supersonic airflow and the four fuel injectors, each inclined at an angle of 15° relative to the airflow direction, a bow shock emerges, resulting in a substantial pressure rise from 40,300 Pa to 85,000 Pa. Subsequently, shock waves propagate and reflect off both the upper and lower walls, leading to a progressive elevation in the averaged pressure throughout the combustor, peaking at 48 kPa. Beyond this juncture, due to the sudden expansion in

cross-sectional area attributed to the presence of the cavity, the pressure experiences a decline to 43 kPa. However, this decline is counterbalanced by the release of heat, initiating a subsequent pressure increase to 94 kPa.

This phenomenon can be explained by the Raleigh law, which postulates that the addition of heat into supersonic flows results in an increase of pressure. Because of the transverse injection of the secondary injectors, the pressure quickly rises to 222 kPa.

Due to the diverging angle of the combustor, the pressure begins to fall to 98 kPa. In some regions, the flow becomes thermally chocked as a result of heat release

6.2. Temperature

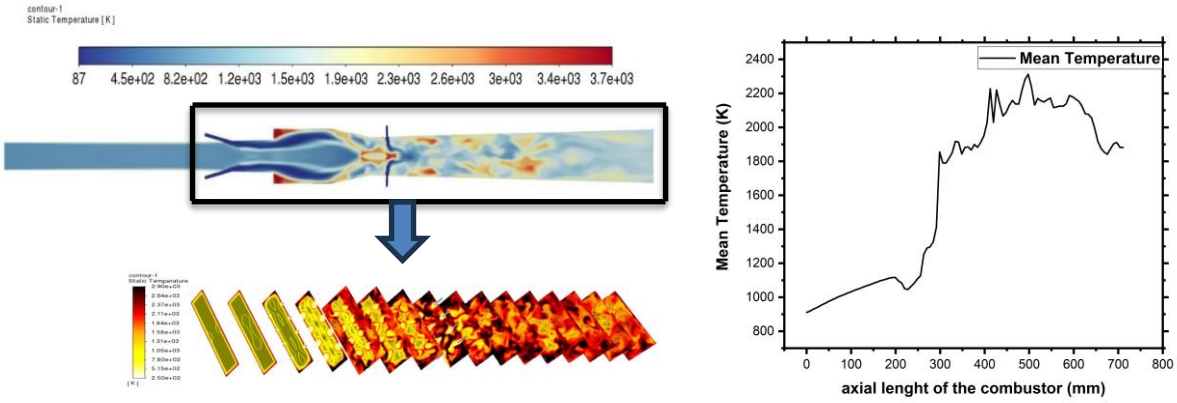

Figure 3. Temperature Contours – Front and transverse planes of the combustor

From the Fig. 3, it is clear that the increase in pressure corresponds to the increase in the temperature in the isolator up to to 1117 K until the primary injection. Later, due to the mixing with the JP4 injection, a slight decrease to 1064 K can be noted. From this point starts again increasing, reaching its maximum of 2300 K. The temperature then remains nearly constant, despite the divergence of the combustion due to heat released from combustion is evident from a trend for H2O mass fraction (see Fig. 6. a).

6.3. Mach Number

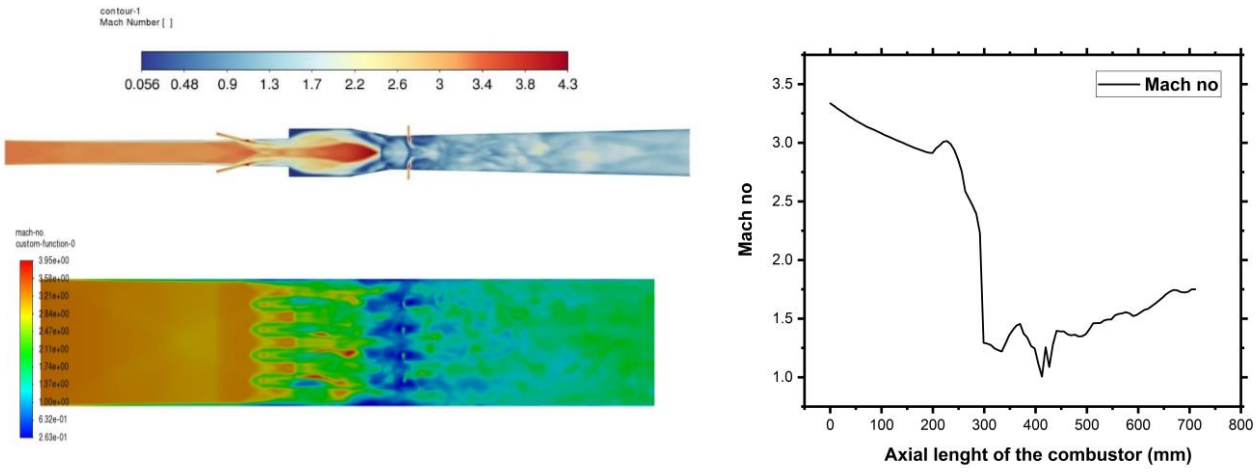

Figure 4. Mach number Contour – Front and top view

From figure 4. It can be noted that a decrease in Mach number due to the rise of oblique shock waves through the combustor until Mach 2.9. Later, due to heat addition from the primary injector, a further decrease in the Mach number can be noted. With the convergence divergence section of the combustor

cavity, we could note a rise in Mach to sonic conditions, which is further changing to supersonic due to the head addition (T0/T*) from cross flow secondary injectors (fig 5). Finally, the divergent part of the combustor allows the Mach number to increase further and establish again the supersonic conditions and reaching M=1.75

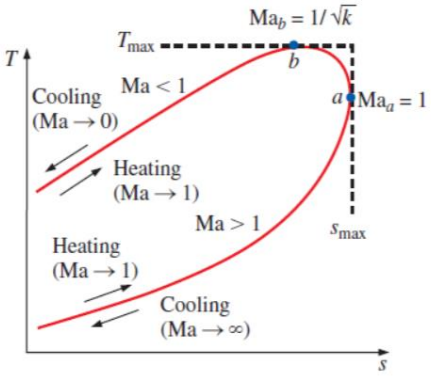

Figure 5. Raleigh flow model (T-S diagram for heat transfer in ducted sections)

6.4. Mass Fraction

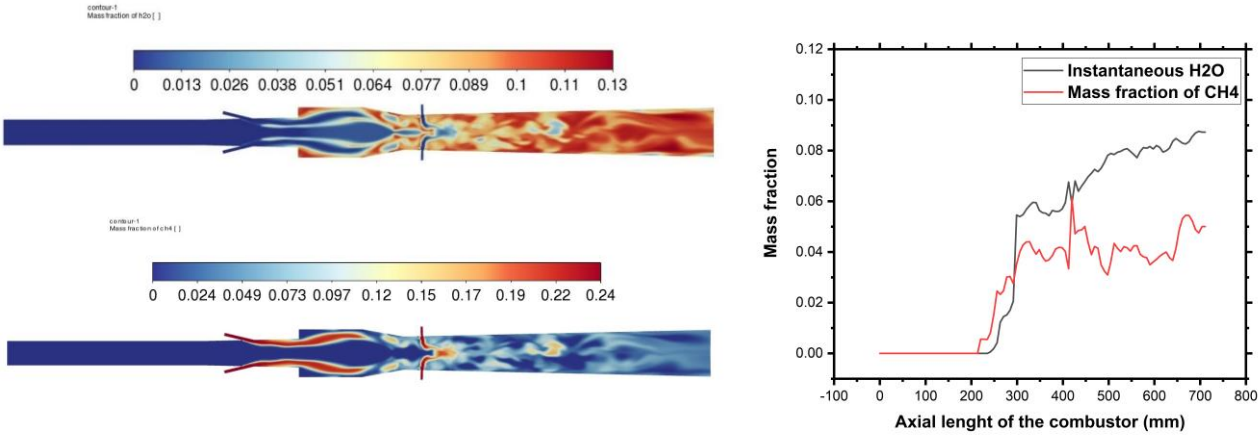

Figure 6. contours of Mass fraction of H_2O and CH_4

Figures 6 show the instantaneous contour of the C2H4 and H2O mass fraction. From the figure, it can be noted that the flame start anchoring upstream of the fuel injection and the primary fuel is almost completely burned into the cavity. The secondary fuel injection, responsible for the high pressure increase due to the bow shock and for the flame ignition, burns efficiently in the second part of the combustor.

6.5. Vorticity and Helicity

Fig 7. shows the vorticity field within the combustor. At the entrance of the combustor the vorticity is practically nil. In the interface region between the incoming flow with the primary injectors, the vorticity increases up to 470000 Hz. The vorticity also contributes to the mixing and combustion within the cavity. The helicity increases from almost 0 to $3x10^8$, confirming the vorticity deformation is mainly due to the streamwise component, that very quickly mix fuel and oxidizer.

Figure 8 shows the vortex structures arising from the primary injection, responsible for the fuel/air mixing and combustion. This result confirm that the cavity downstream of the inclined injection, coupled with the cross flow secondary injection is able to ensure a good mixing and combustion efficiency.

The Q criterion shows that the deformation of the vortex structures is mainly related to the streamwise vorticity

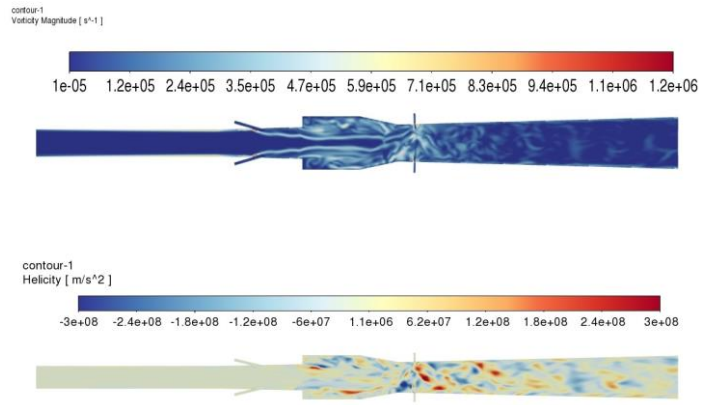

Figure 7. Instantaneous vorticity in the transversal plane passing through the centre of the injectors (top) and the corresponding (b) Helicity (bottom)

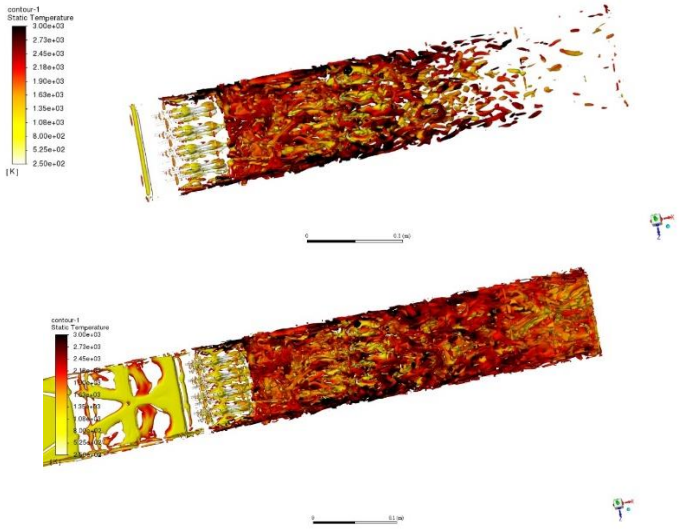

Figure 8. ***Q=0.1 and Q=100 Isosurface coloured by Instantaneous temperature***

7. Conclusion:

In this paper large eddies Simulations have been performed to investigate the interaction between the shock waves, boundary layer and the fuel injections were studied numerically on the HIFiRE-2 scramjet combustor. Instantaneous LES results at t=0.0024s and the mean values were analysed. The Q criterion has shown that the deformation of the vortex structures is mainly related to the streamwise vorticity. Mixing times have been estimated of the order of 10-5 10-6 s, i.e., almost two orders of magnitude shorter than the residence time. Due to this efficient mixing, the combustion efficiency, has found to be of about 97%, calculated considering the unburned mass at the outlet with respect to the injected mass.

Total pressure losses in hot flow are 84% while in cold flow, the total pressure loss is 72.41%, with a total pressure loses addition of about 12%. This suggests that new configuration with swirling injectors,

different injector's locations and angles, different cavity geometries, should be investigated to reduce total pressure losses without decreasing the mixing efficiency

References

[1] Eunju Jeong, Sean O'Byrne, In-Seuck Jeung, and A. F. P. Houwing – "The Effects of Fuel Injection Location on Supersonic Hydrogen Combustion in a Cavity-Based Model Scramjet Combustor " Energies **2020**, 13, 193; doi:10.3390/en13010193

[2] Zun Cai, Xiao Liu, Cheng Gong, Mingbo Sun, Zhenguo Wang, Xue-Song Bai- " Large Eddy Simulation of the fuel transport and mixing process in a scramjet combustor with rear wall-expansion cavity" http://dx.doi.org/10.1016/j.actaastro.2016.05.010

[3] Obula Reddy Kummitha – " Numerical analysis of passive techniques for optimizing the performance of scramjet combustor". http://dx.doi.org/10.1016/j.ijhydene.2017.01.148

[4] Frank W. Barnes, Corin Segal – "Cavity-based flame holding for chemically reacting supersonic flows ".http://dx.doi.org/10.1016/j.paerosci.2015.04.002

[5] Vignesh Ram Petha Sethuraman, Yosheph Yang, and Jae Gang Kim Interaction of shock train with cavity shear layer in a scramjet isolator. Phys. Fluids 35, 036111 (2023); doi: 10.1063/5.0137481

[6] Bruno, C., Ingenito, A. (2021), Some Key Issues in Hypersonic Propulsion, Energies 2021, 14(12), 3690; https://doi.org/10.3390/en14123690.

[7] Ingenito, A.; Bruno, C.; Mixing and combustion in supersonic reactive flows, 44th AIAA/ASME/SAE/ASEE Joint Propulsion Conference and Exhibit, 2008, 978-156347943-4 10.2514/6.2008-4574.

[8] Vatsalya Sharma, Vinayak Eswaran, Debasis Chakraborty, - "Effect of location of a transverse sonic jet on shock augmented mixing in a SCRAMJET-engine" https://doi.org/10.1016/j.ast.2019.105535

[9] Namrata Bordoloi, Krishna Murari Pandey, Mukul Ray, Kaushal Kumar Sharma – "Impact of passive fuel injections techniques in the flow field of the scramjet-combustor" https://doi.org/10.1016/j.ijft.2022.100225

[10] K. M. B. N. Pandey, "Numerical simulation of a hydrogen fueled scramjet combustor at Mach 1.5 using sturt injectors at Mach 2.47 air speed.," in Proceedings of the ASME 2013 International Mechanical Engineering Congress and Exposition IMECE2013 November 15-21, 2013, San Diego, California, USA, 2016, pp. 1–13

[11] N. Bordoloi, K.M. Pandey, K.K. Sharma, Numerical investigation on the effect of inflow Mach numbers on the combustion characteristics of a typical cavity-based supersonic combustor, Math. Probl. Eng. 2021 (2021) - https://doi.org/ 10.1155/2021/3526454

[12] J.V.S.S. Moorthy, B. Rajinikanth, B.V.N.N. Charyulu, G.Amba Prasad Rao, G.A. P. Rao, Effect of ramp-cavity on hydrogen fueled scramjet combustor, Propuls. Power Res. 3 (1) (2014) 22–28, https://doi.org/10.1016/j.jppr.2014.01.001

[13] K.M. Pandey, Gautam Choubey, Fayez Ahmed, Dilbahar Hussain Laskar, Pushpdeep Ramnani – "Effect of variation of hydrogen injection pressure and inlet air temperature on the flow-field of a typical double cavity scramjet combustor"

[14] Relangi N., Ingenito A., Jeyakumar S., The investigation of inclined aft wall cavities in a circular scramjet combustor, International Journal of Engine Research, 2022.

[15] Relangi N., Ingenito A., Jeyakumar S. (2021). The implication of injection locations in an axisymmetric cavity-based scramjet combustor. ENERGIES, vol. 14, ISSN: 1996-1073, doi: 10.3390/en14092626

[16] ANSYS Fluent software. https://www.ansys.com/products/fluids/ansys-fluent